Measurement Methods of Electron Emission Over a Full Range of Sample Charging

R. Hoffmann and J.R. Dennison

***Abstract*— Spacecraft charging codes require accurate models of electron yields as a function of accumulated charge to correctly predict the charge build up on spacecraft. The accumulated charge creates equilibrium surface potentials on spacecraft resulting from interactions with the space plasma environment. There is, however, a complex relation between these emission properties and the charge built up in spacecraft insulators.**

This paper focuses on different methods appropriate to determine the fundamental electronic material property of total electron yield as the materials accumulate charge. Three methods for determining the uncharged total yield are presented:

(i) The DC Continuous Beam Method is a relatively easy and accurate method appropriate for conductors and semi-conductors with maximum total electron yield σ_{max}<2 and resistivity ρ<10^{17} Ω-cm.

(ii) The Pulse-Yield Method seeks to minimize the effects of charging and is applicable to materials with σ_{max}<4 and ρ up to >10^{24} Ω-cm.

(iii) The Yield Decay Method is a very difficult and time consuming technique that uses a combination of measurement and modeling to investigate the most difficult materials with σ_{max}>4 and ρ up to >10^{24} Ω-cm.

Data for high purity polycrystalline Au, Kapton™ HN and CP1™ polyimides, and polycrystalline aluminum oxide ceramic are presented. These data demonstrate the relative strengths and weaknesses of each method, but more importantly show that the methods described herein are capable of reliably measuring the total electron yield of almost any spacecraft material.

***Index Terms*—Electron Yield, Insulator, Measurement Techniques, Spacecraft Charging.**

I. Introduction

The central theme of spacecraft charging is how spacecraft interact with the plasma environment to cause charging. Spacecraft materials accumulate negative or positive charge and adopt potentials in response to interactions with the plasma environment. A material's electron emission and total electron yield, σ, (defined as the ratio of net electron flux out of a material to the incident electron flux), determines how quickly net charge accumulates in spacecraft components in response to incident electron, ion, and photon fluxes. The total yield, $\sigma \equiv \eta + \delta$, is commonly written as the sum of backscattered, η, and secondary electron, δ, yields,. The material resistivity, ρ, determines how quickly that charge is dissipated. In a thin film capacitor approximation, the decay time, $\tau = \varepsilon_0 \varepsilon_r \rho$, is linearly proportional to ρ; ε_r is the relative dielectric constant of the material. Due to their high mobility, incident electrons from the space plasma play a more significant role in electron yield and in resulting spacecraft charging than do positively charged ions. For this reason, the focus of this study is on electron interactions; ion and photon interactions are neglected.

There is a complex relation between the electron emission properties of insulating materials and the incident and accumulated charge in spacecraft insulators. Insulating materials generally exhibit higher yields than conducting materials, and accumulated charge cannot be easily dissipated. Therefore, insulating materials can be very efficient at collecting and storing charge. This becomes a very dynamic problem, as electron emission in insulators is complicated by the fact that the emission mechanisms themselves can be influenced by accumulated surface and bulk charge. In addition, the conductivity of the material can be modified by the energy deposited by the incident electron [1]. The net charge that a material will obtain is dictated by the complex interplay of all of these processes.

II. Yield Measurement Methods

This work outlines three methods developed by the Utah State University (USU) Materials Physics Group (MPG) to measure the electron-induced electron yield of materials with resistivities ranging from conductors with $\rho \rightarrow 0$ to extreme insulators with $\rho \rightarrow \infty$ and with maximum total yields ranging from σ_{max}<1 to σ_{max}~40. A combination of these methods are shown to span the full spectrum of spacecraft material testing that needs to be performed for full inclusion of electron yields into modeling codes developed to predict spacecraft charging.

A. DC Yield Method

A DC method with a continuous, low-current beam of electrons of energy E_b is used effectively to measure electron emission and electron yield from conductors, semiconductors, and modest insulators with ρ<10^{17} Ω-cm. Discharge times are τ<10^4 s, comparable to emission measurement times. Charge added to or removed from the sample, via electron emission, can be rapidly replaced by connecting the sample to ground [2, 3]. The fully encased hemispherical grid retarding field detector used at USU (see Fig. 1) facilitates high accuracy measurements of absolute yields (on the order of ±2%); such

This study was partially funded by the NASA Solar Probe Mission through the Johns Hopkins University Applied Physics Laboratory and by the NASA Space Environments and Effects program.

Ryan Hoffmann is a Research Physicist at the Air Force Research Laboratory (AFRL) in Albuquerque, NM 87111 USA (email: Ryan.Hoffmann@Kirtland.af.mil).

JR Dennison is a professor with the Materials Physics Group in the Physics Department at Utah State University in Logan, UT 84322 USA (e-mail: JR.Dennison@usu.edu).

very high accuracy measurements are not possible using other common instrumentation and methods [4, 5]. It also allows the application of a separate bias to each of the discrete elements of the detector. These biases allow for the discrimination of secondary (SE) and backscatter electrons (BSE) and measurement of electron emission spectra, in contrast to the more typical method of only measuring the biased sample current. The individually biased elements of the HGRFA detector also allow for extensive instrument characterization and calibration. A thorough discussion of the DC system and methods is given by Thomson [5] and others [4, 6].

Two electron sources provide electron energy ranges from ~20 eV to ~30 keV and incident electron currents (0.1 to 500 nA or <10 pA/cm^2 to 50 µA/cm^2 current densities) with pulsing capabilities ranging from 10 ns to continuous emission. The low-energy electron gun (Staib, Model EK-5-S) operates at incident electron energies of ~20 eV to 5000 eV with a maximum beam current of ~100 nA and a <0.1 mm minimum diameter beam spot. The high-energy electron gun (Kimball Physics, Model ERG-21) operates at incident electron energies of 3.5 keV to 30 keV with a typical beam current of ~20 nA and a 500 µm minimum diameter beam spot.

For electron yield measurements on conductors, a continuous incident beam is directed on the sample and currents from the detector (see (A) in Fig. 1(b)), suppression grid (B), inner-grid (C), stage (D), and sample (E) are measured using custom electrometers [4]. A 50 V bias on the detector, relative to the suppression grid, is maintained to insure collection of all electrons that are able to penetrate the grids. Grounding the grids through the electrometer facilitates the measurement of the total yield σ by allowing all emitted electrons to be collected. A -50 V bias relative to the sample is then applied to the suppression grid allowing only the BSE with energies >50 eV to reach the detector, thus determining the BSE yield. The secondary yield is calculated as the difference between the BSE and the total yields.

Figure 2 shows a representative conductor yield curve for polycrystalline Au [7]. E_1 and E_2 are the first and second crossover energies at unity total yield. The yield peak, σ_{max}, is the maximum yield and occurs between the crossover energies at E_{max}.

B. Effects of Charge Accumulation on Yields

When a material is exposed to high-energy electron irradiation, electrons emitted from the material have a range of emission energies from 0 eV up to the incident electron energy, E_b. Emitted electrons with energies <50 eV are customarily assumed to be SE's originating from within the material. The escape energies of SE's depend on their production depth, as well as the energy-loss mechanisms and surface potential barriers experienced before exiting the material, but 50 eV serves as a convenient demarcation as long as the incident electrons E_b>50 eV. BSE's are electrons that quasielastically scatter from the material and have energies up to E_b. Again, a convenient demarcation for BSE is that they have energies >50 eV; this is a reasonable convention as long as the incident beam E_b>50 eV.

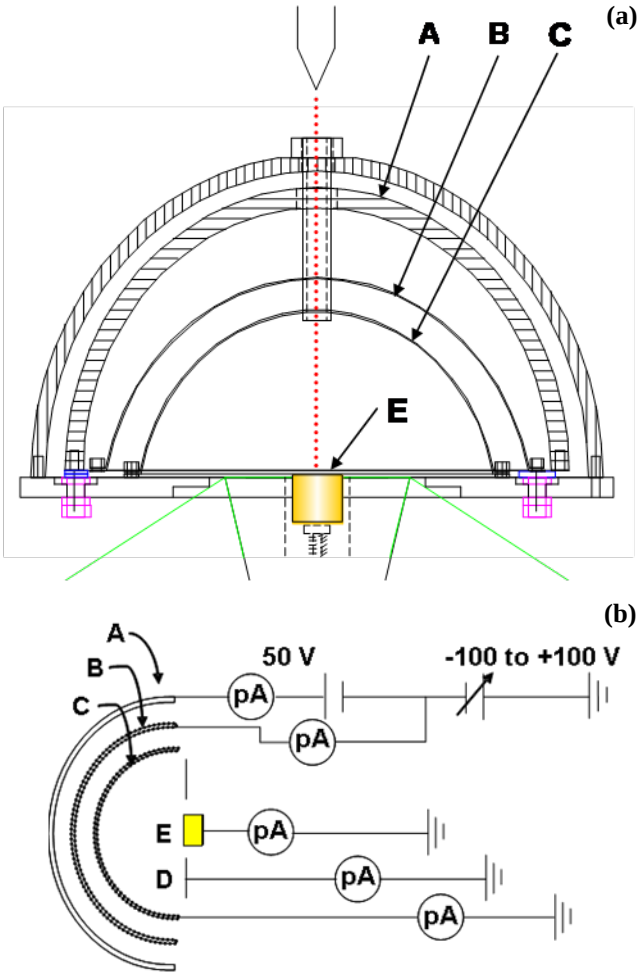

Fig. 1. (a) Simplified cross-section of Hemispherical Grid Retarding Field Analyzer (HGRFA) used for electron emission detection in all methods. (b) Schematic of HGRFA. Electron beam (red dashed line) incident on sample. (A) Solid hemispherical collector. (B) Bias grid used to discriminate electron energies coming from the sample. (C) Inner grid used to provide a uniform electric field and shield from unwanted edge effects. (D) Sample stage comprises the hemispherical shield and sample mounting platform. (E) The electrically isolated sample is held in the center of hemisphere.

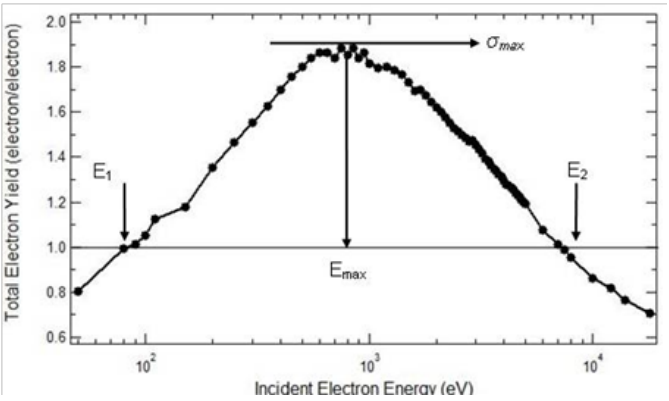

Fig. 2. Total electron yield of polycrystalline Au as a function of incident energy. Data were taken using the DC Yield Method. Note the logarithmic energy axis. Also note the crossover energies E_1 and E_2 and the peak yield σ_{max} at energy E_{max}.

Figure 3 shows the pronounced effects of accumulated charge on total, secondary and backscattered yield measurements of modestly insulating materials such as CP1™,

even when low fluence pulsed methods are employed. Several distinct regions (Zones 1-6) are identified for the curves:

Zone 1: $E_b<E_1$, where $\sigma<1$. σ, η and δ are not appreciably affected by the small negative surface charge.

Zone 2: $E_1>E_b>E_2$, where $\sigma>1$. σ and δ are depressed due to small positive sample charging and the subsequent re-attraction of some low energy SE's. η is unaffected by the relatively small positive surface voltage, V_s.

Zone 3: $E_2<E_b\lesssim$1200 eV, where $\sigma<1$. In Zones 3, 4 and 5 σ (and δ) is above the true uncharged total yield curve depicted by the green line in Fig. 3. This results from "extra" emission of SE's from the thin electron depletion region, due to the large electric field from the negative layer deposited at penetration depth R. For Zone 3, R is less than or approximately equal to the range of most SE [8]. In Zone 3, η remains nearly constant, as few SE gain enough energy from the small negative surface potentials to be counted as BSE. Recall that the emission energy of true backscattered electrons that originate in the electron beam—which are first accelerated (decelerated) by a positive (negative) surface potential as they enter the material, and then decelerated (accelerated) by the same surface potential as they leave—is unaffected by surface potential; this is in contrast to true secondary electrons that originate within the material and are only decelerated (accelerated) by a positive (negative) surface potential.

Zone 4: 1200 eV$\lesssim E_b\lesssim$1500 eV. σ is enhanced because of the increasing negative surface potential and η begins to increase as some higher energy SE's are accelerated to BSE energies (>50 eV).

Zone 5: 1500 eV$\lesssim E_b\lesssim$6000 eV. Most of the SE's are accelerated to BSE energies by large negative surface potentials, $|V_s|\gtrsim$50.

Zone 6: $E_b\gtrsim$6000 eV. σ largely returns to the idealized uncharged green yield curve; few SE produced in the depletion region gain sufficient energy from the electric field due to the embedded charge, which decreases as the electron range increases with increasing incident energy. The BSE yield is almost equal to σ, as essentially all SE have been accelerated and converted to BSE.

C. Pulsed Yield Method

The system employed at USU to measure electron emission from insulators (see Fig. 4 of Ref. [9], and especially Ref. [7] for details) uses the same fully encased HGFRA detector and electron sources employed for DC measurements, in concert with methods to control the deposition and neutralization of charge [4, 10-12]. This is accomplished by minimizing the amount of charge used in the probe beam by using a pulsed, low-fluence beam rather than the continuous beam used for conductors. Typically, charge deposition is minimized by using a low-current beam focused on a sample area of ~2.3±0.2 mm^2 that is delivered in short pulses of ~5 μsec. The pulsed system uses custom detection electronics with fast (1-2 μs rise time) sensitive/low noise (10^7 V/A / 100 pA noise level) ammeters [5, 10]. Great care was taken to minimize overall system noise to reach the capabilities listed above. These efforts have included AC power filtering, increased

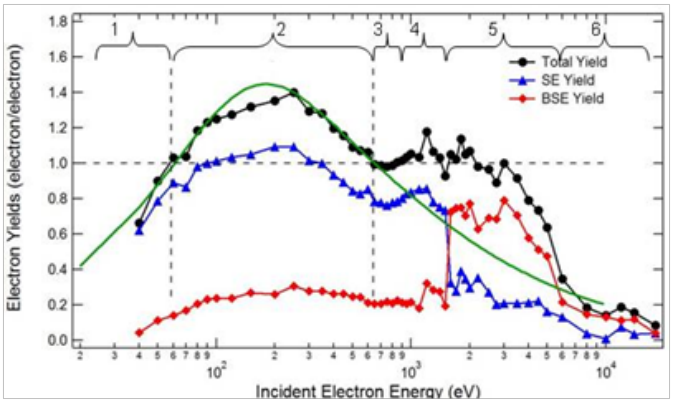

Fig. 3. Total (**black dots**), secondary (**blue triangles**) and backscattered (**red diamonds**) electron yields for CP1™ (a modified, more conductive form of polyimide) showing six distinct regions of charging behavior. The thick (**green**) curve is the estimated "intrinsic" or uncharged yield curve.

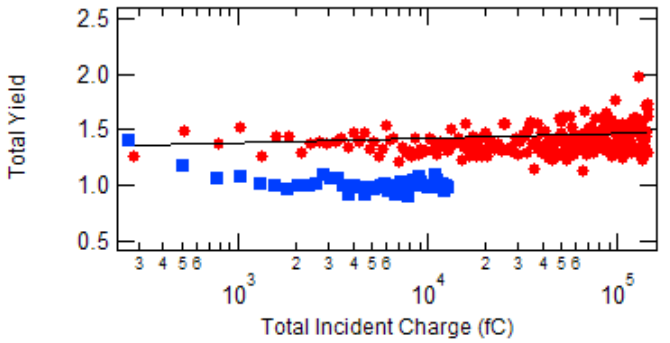

Fig. 4. To show the effectiveness of low fluence pulsing coupled with low energy flooding, two sets of data were taken on Kapton HN™ at 200 eV incident energy, one with charge neutralizing low energy electron flooding (**red dots**) and one without flooding (**blue squares**).

cable shielding, plus identification and removal of problematic noise sources and ground loops. The system is capable of measuring an incident pulse of ~$6\cdot10^3$ electrons/mm^2. The charge density from such a pulse is ~$6\cdot10^6$ electrons/mm^3, assuming an isotropic distribution of electrons in the material from the surface to the penetration depth of ~1 μm [8]. For perspective, this electron density can be compared to that of intrinsic silicon with a free carrier density of ~$6\cdot10^9$ electrons/mm^3.

Pulsing the beam minimizes the deposited charge; however, insulators can store charge for a very long time. Even using a pulsed, low-fluence electron probe pulse, after repeated pulses charge accumulates in the material and can cause an unacceptable modification to the yield measurements. To counter this, a low energy (3 eV) defocused flood gun is used to dust the surface with electrons and neutralize positive charge accumulation. The electron flood gun used for charge neutralization can also provide a focused low-energy (1 eV to 200 eV) source. The data in Fig. 4 show the modification of the total yield for successive pulses, with and without low energy electron flooding. Note that the unneutralized yield curve (blue squares in Fig. 4) asymptotically approaches unity, as the sample charges and re-attracts successively more emitted SE. The neutralized yield (red dots in Fig. 4) remains nearly constant, consistent with minimal net charge accumulation. A slight increase observed in the neutralized

yield curve is attributed to increased defects generated by the incident radiation dose. This clearly demonstrates that the electron flood charge neutralization method is effective.

Because surface charging is a function of incident flux and not simply incident fluence, a careful characterization was performed on the electron sources. By measuring the beam profile, and establishing controller settings for the full energy range, we have ensured that the spot size (and consequently deposited charge density) is consistent at 1.7±0.3 mm full width at half maximum over the entire yield curve. This is a departure from the work previously performed with this instrument, where the beam spot size ranged from 0.3 to 1.5 mm in diameter [5, 7].

Minimizing the incident charge fluence (~5 fC/mm^2) with low flux (~1 nA/mm^2) and short duration pulses (~5 μs) and discharging the material after every pulse to prevent charge accumulation has proven to be effective when the material has both a moderate yield and high resistivity. The data for Kapton HN™ in Fig. 5 show total, SE, and BSE yield curves taken with the pulse yield system. This material has a high resistivity of 10^{19} Ω-cm, with a corresponding charge decay time of $>10^6$ s. Since this decay time is much longer than the few hours required to measure a pulsed yield curve, the material is effectively a perfect charge integrator. There is no evidence of charge modified yield in Fig. 5 below $E_b<E_2$. Above this energy, negative surface potentials accelerate the SE's peaked at ~3 eV (see, *e.g.*, Fig. 6) to energies >50 eV and these electrons begin to be measured as BSE's. This is to be expected, because our electron flood discharge methods do not dissipate negative charge accumulation.

The upper and lower resistivity bounds for the Pulsed Yield Method are relatively easy to establish. The Pulsed Yield Method is applicable to materials with resistivities approaching zero for the lower bound. However, this method is not often used to test low resistivity materials, as it generally has greater error and is much more time intensive than the DC Yield Method.

The Pulsed Yield Method can be effectively used for materials with resistivities approaching infinity. In practice, this upper limit is set by the isotropic extra-galactic cosmic background radiation flux, with particles of high enough energy that they penetrate the atmosphere and not be appreciably attenuated by a vacuum test chamber wall or a spacecraft; this flux is essentially the same in all space environments or terrestrial laboratories [13]. This cosmic radiation excites some electrons into the conduction band and so produces a constant lower bound to conductivity from radiation induced conductivity (RIC). A crude calculation—assuming a worldwide average natural background radiation dose for a human being from the cosmic ray background of ~0.3 mSv per year [14] and a typical biological radiation weighting factor of 1 Gy/Sv—predicts an annual dose of ~46 mRad and an average dose rate of $1•10^{-9}$ Rad/s. For typical polymers at room temperature, this corresponds to a cosmic background RIC of $\sim 4•10^{-23}$ (Ω-cm)$^{-1}$ [15]; this is comparable to thermal Johnson noise for typical materials and test apparatus. For typical polymers at 100 K, RIC from the cosmic background is four orders of magnitude less than at

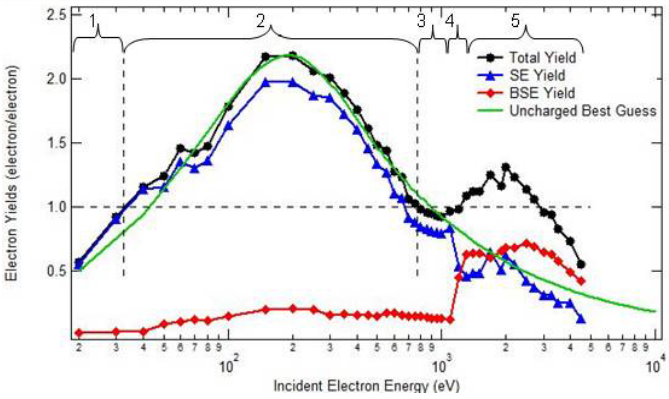

Fig. 5. Total (**black dots**), secondary (**blue triangles**) and backscattered (BSE) (**red diamonds**) electron yield curves for Kapton HN™ taken with the pulsed yield system employing both low-fluence pulses and low-energy flooding. The thick (**green**) curve is the estimated "intrinsic" or uncharged yield curve. There is no evidence of charging up to ~1100 eV, where the BSE yield abruptly increases. This is an indication that SE's are being accelerated to ≳50 eV due to negative potential within the material.

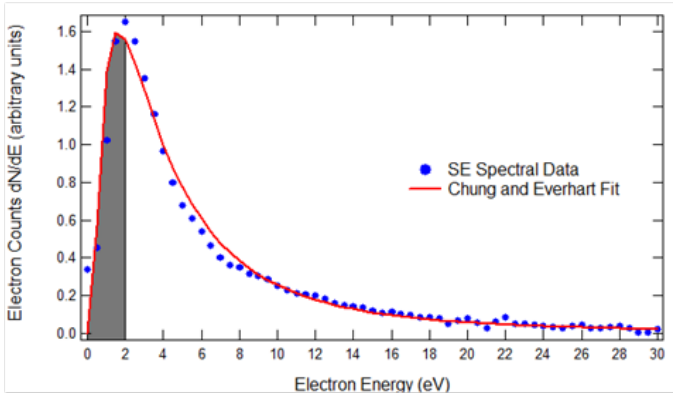

Fig. 6. Secondary Electron (SE) emission spectra of polycrystalline Al_2O_3 fit with a model developed by Chung and Everhart [17]. The gray area represents the fraction of SE that would be re-attracted to the surface with a +2 V surface potential.

room temperature [13, 15]; Johnson noise is an order of magnitude less. Therefore, an upper limit on measurable room temperature resistivity for any materials can be set at ~10^{24} Ω-cm, with a corresponding charge decay time of ~10^2 yr.

The limits of the Pulsed Yield Method in terms of total yield are illustrated by the yield curve taken for polycrystalline aluminum oxide ceramic in Fig. 7. These bounds are unique to each pulse yield system as they are dependent on the signal-to–noise ratio inherent in the system. As can be seen from the blue data in Fig. 7, Al_2O_3 has a much higher yield than that of Kapton HN™, and as E_b approaches ~200 eV, the yield increases until $\sigma>4$, above which σ begins to fall off. At this point, the charge contained in each individual pulse is enough to cause a significant positive potential in the irradiated portion of the sample, and as a result SE's are re-attracted to the surface and the total yield is reduced toward unity. As E_b increases, the effect continues until the yield drops to ~1, at which point the probe pulse is no longer causing significant charging. This sets the upper limit of applicability for the Pulsed Yield Method as $\sigma_{max}<4$; this could be increased if the incident pulse could be made smaller by further reducing the signal-to-noise ratio inherent in the system. As a lower bound

for total yield this method is capable of measuring yields approaching zero.

D. Composite Yield Method

The Composite Yield Method or Yield Decay Method combines the low fluence Pulsed Yield Method and emission spectra data to determine the yield curves of high yield insulators that still charge under low current pulses. The Composite Yield Method overcomes this by measuring the response of the yield to incident charge and then using modeling to extrapolate to a minimally charged condition [16]. It is applicable to high yield insulators with typical yield $\sigma_{max}>4$ and $\rho \rightarrow \infty$ (Ω-cm). An overview of the concept is provided here; for a full explanation see Hoffmann [7, 16].

Measured emission spectra for Al_2O_3 at 200 eV are shown in Fig. 6, along with a fit based on the Chung-Everhart model for the differential of the energy distribution curve for SE emission, $dN(E)/dE$ [17]. Between the total-yield crossover energies, E_1 and E_2, the magnitude of insulator charging is positive (since $\sigma>1$), and due to the re-attraction of low energy electrons, the insulator attains a steady-state surface potential of just a few volts positive. This positive charging increases the insulator surface potential barrier by an amount eV_s. Hence, the resulting SE yield emitted from a positively charged specimen can be expressed as an integral of the uncharged spectrum (taken at the same incident energy)

$$\int_{eV_s}^{50eV} \frac{dN(E;E_o)}{dE} dE + 1 = \delta(E_o;V_s) + \eta_o = \sigma(E_o;V_s)$$

with the integration limits extending from the positive surface potential up to the arbitrary 50 eV limit of SE energy [18, 19]. $\eta(E_b) \equiv \eta_o$ is assumed to be unaffected by the built up potential, because η is roughly constant above ~150 eV.

An analytical solution to this integral gives an expression that describes the re-attraction of SE's to the surface of a positively charged sample:

$$\sigma(E_o;V_s) = \frac{k}{6E_o}\left[h(eV_s;\chi) - h(50eV;\chi)\right] + 1,$$

where

$$h(\alpha;\chi) \equiv \frac{3\alpha + \chi}{(\alpha + \chi)^3},$$

k is a material dependant proportionality constant, χ is the insulator electron affinity, and α is an arbitrary energy at which h is evaluated [5]. The positive surface charging inhibits the escape of lower-energy SE's, thus suppressing the lower-energy portion of the SE spectrum (represented by the shaded area in Fig. 6). Consequently, only the unshaded area of the electron energy spectrum (above eV_s) contributes to the charged electron yield.

This yield decay model describes the modification of the total yield as a response to surface potential. Efforts are currently underway to concurrently measure the surface potential directly [20], however the data presented here rely only on the capability to measure the incident and return flux. To relate the surface voltage to the incident flux, the Dual Dynamic Layer Model (DDLM) [21-24] has been employed to establish the relationship between the surface voltage and incident electron flux. This allows us to model the evolution of the total yield as a function of the measured incident flux or as a function of the surface potential (calculated using the DDLM). These data and fit are shown in Fig. 8.

Using the Composite Yield Method, the total yield is measured as total incident flux is increased and then these data are fit with a physics-based empirical model as the yield decays to unity. This fit then allows the extrapolation of the yield to incident fluxes approaching negligible charge, the so-called "intrinsic" yield. This extrapolation is only valid for the total yield at the incident energy of the decay curve. To measure the complete total yield curve, data must be taken for a spectrum of incident energies, fit with the yield decay model, and then extrapolated to a 0 V surface potential. These data are shown in Fig. 9 (green squares). The discrepancies between the measured data and the green "intrinsic" yield

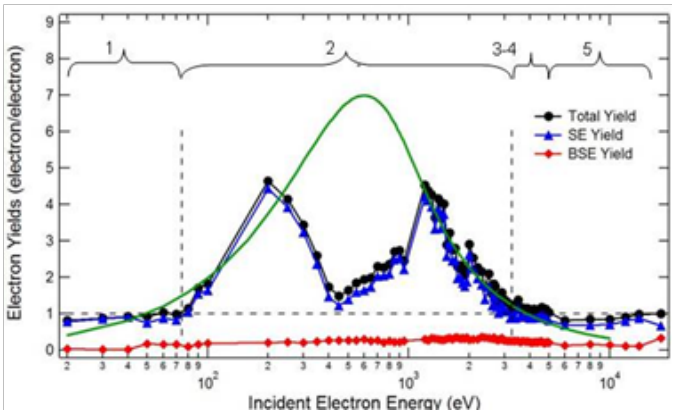

Fig. 7. Total (**black dots**), secondary (**blue triangles**) and backscattered (BSE) (**red diamonds**) electron yield curves of polycrystalline Al_2O_3 taken using the Pulsed Yield Method system employing both low-fluence pulses and low-energy flooding and predicted with the Composite Yield Method. The dual peak behavior between the crossover energies is evidence of positive charging, as a significant fraction of the SE's are re-attracted to the surface. The thick (**green line**) curve is the estimated "intrinsic" or uncharged yield curve.

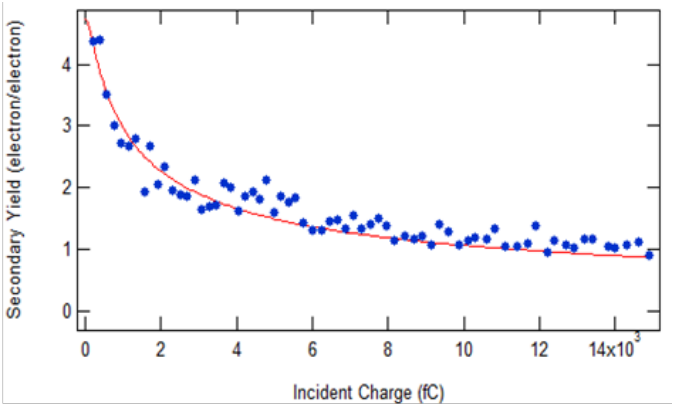

Fig. 8. Measured secondary electron yield of polycrystalline Al_2O_3 at 200 eV as the material charges. The fit to the yield, based on the integrated Chung and Everhart model [17], is used to extrapolate the yield to negligible incident charge [7].

curve show where the pulsed yield method failed due to charging of the polycrystalline aluminum oxide.

This method is very time consuming and difficult to implement, but it has proven capable of measuring materials with both high yield >4 and high resistivity $>10^{16}$ Ω-cm. This ability is due to the fact that this method does not attempt to minimize and dissipate charging as in the pulse yield method; rather it takes advantage of charging and models the evolution of the total yield, thus allowing predictions of an uncharged yield. To apply this method requires that the material must have a charge decay time constant of >4 s (the experimental time frame to acquire one yield measurement at a given incident energy)—with a corresponding resistivity $>10^{12}$ Ω-cm—such that charge is allowed to accumulate on the surface between measurements. Since this method relies on a model of positive surface potential re-attraction of SE's, it cannot be used to measure a total yield of ≤1. The upper bound for total yield is set by the minimum flux contained in each probe pulse, or in other words how quickly the material charges and consequently how many points there are on the yield decay curve before it reaches unity. Based on this, we project that the Composite Yield Method can be applied to materials with $\sigma_{max} \leq 40$.

III. Summary

The parameters of maximum total yield and conductivity dictate the charging susceptibility. Figure 10 depicts the demonstrated and predicted capabilities of the three methods described here. These methods have demonstrated broad applicability to a wide variety of materials. Further, we predicted that these methods can be used to measure materials with any degree of charging susceptibility, from conductors (low-yield; low-resistivity) to diamond (high-yield; high-resistivity). The methods described herein are applicable over the entire range of both total yield (from 0 to 40) and resistivity (from 0 Ω-cm to $>10^{24}$ Ω-cm) [7].

In the spacecraft charging community much attention is paid to material resistivity or in other words how the material stores charge. Because of the difficulty in measurement, yield is often neglected as a significant contributor to the effect of spacecraft charging. Instead, we in the spacecraft charging community, tend to focus on resistivity because of its relative ease of measurement and the ability of the resistivity parameter to be easily modified in code models of specific applications. A primary reason for this one-sided approach is the fact that very often consistent, reliable, and repeatable yield data are not available in the literature, especially for insulators. The methods to acquire these data simply did not exist in the past, so researchers were forced to use poor quality yield data as inputs in charging codes. The methods and capabilities described herein have completely overcome this deficiency. We have demonstrated the ability to measure uncharged yields from polymers such as Kapton HN™ as well as ceramics such as polycrystalline aluminum oxide. Further we predict that it will be possible to use these methods on even the most challenging high yield materials, the so-called negative electron affinity materials such as diamond and certain doped cover-glass materials.

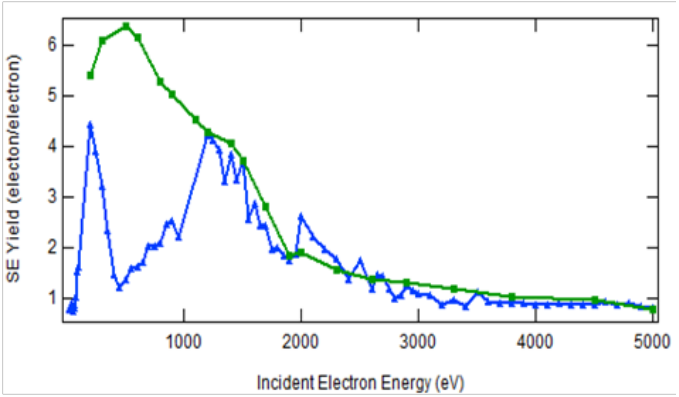

Fig. 9. By producing many yield decay curves like Fig. 8 and extrapolating them to zero incident charge, we obtain the "intrinsic" yield curve for high yield insulators(**green squares**) such as polycrystalline Al_2O_3 from the measured total yields (**blue dots**) [16].

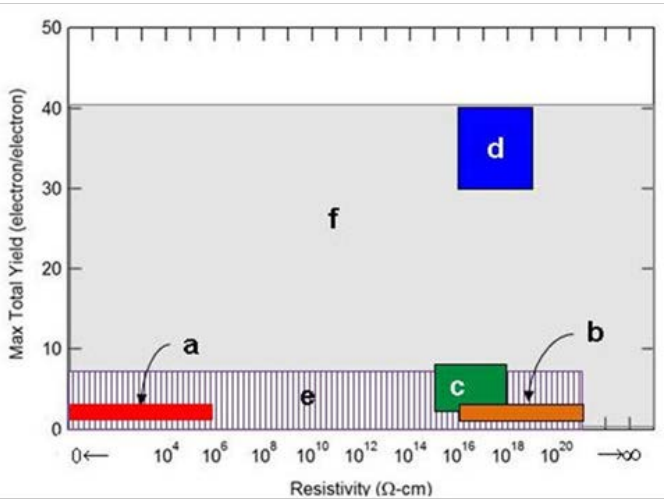

Fig. 10. Description of measurable ranges of total electron yields of materials.

a) Low resistivity conductors and semiconductors, with $\sigma_{max}<2$ and $\rho<10^6$ Ω-cm. (red solid)
b) Low yield insulators, such as polymers (*e.g.*, Kapton or Mylar), with $\sigma_{max} \lesssim 2$ and 10^{16} Ω-cm$\lesssim \rho \lesssim 10^{21}$ Ω-cm. (orange solid)
c) High yield insulators, such as metal oxide ceramics (*e.g.*, Al_2O or MgO), with $1.5 \lesssim \sigma_{max} \lesssim 8$ and 10^{15} Ω-cm$\lesssim \rho \lesssim 10^{18}$ Ω-cm. (green solid)
d) Extremely high yield negative electron affinity materials (*e.g.*, diamond), with $30 \lesssim \sigma_{max} \lesssim 40$ and 10^{16} Ω-cm$\lesssim \rho \lesssim 10^{19}$ Ω-cm. (blue solid)
e) Range of material testing conducted to date by the USU Materials Physics Group, with $\sigma_{max}<8$ and $\rho<10^{21}$ Ω-cm. (purple hatched)
f) Potential range of applicability of currently developed test methods (light grey).

Acknowledgment

We acknowledge the many members of the USU Materials Physics Group who have contributed over the last decade to the development and application of the techniques discussed in this paper. We especially recognize Neal Nickels, Albert Chang and Clint Thomson.

References

[1] J.A. Roth, R. Hoffmann, J.R. Dennison, and J. R. Tippetts, "Effects of Radiation Induced Conductivity on Electrostatic Discharge in Insulating Materials," Paper Number: AIAA-2009-3527, *Proc. of 1st AIAA Atmospheric and Space Environ. Conf.*

2009.
[2] E. Baroody, "A theory of secondary electron emission from metals," *Phys. Rev.*, vol. 78, pp. 780-787, 1950.
[3] H. Bruining and J. De Boer, "Secondary Electron Emission: Part I. Secondary Electron Emission of Metals," *Physica*, vol. 5, pp. 17-30, 1938.
[4] N. Nickles, "The Role of Bandgap in the Secondary Electron Emission of Small Bandgap Semiconductors: Studies of Graphitic Carbon," Ph.D. Dissertation, Dept. Physics, Utah State University, Logan, UT, 2002.
[5] C. Thomson, "Measurements of the Secondary Electron Emission Properties of Insulators," Ph.D. Dissertation, Dept. Physics, Utah State University, Logan, UT, 2004.
[6] W.Y. Chang, J.R. Dennison and P. Judd, "Measurements of Electronic Properties of Conducting Spacecraft Materials with Application to the Modeling of Spacecraft Charging," Paper AIAA-2000-0870, *Proc. 38th AIAA Meeting on Aerospace Sci.*, (Reno, NV, 2000)..
[7] R. Hoffmann, "Electron-Induced Electron Yields of Uncharged Insulating Materials " M.S. Thesis, Dept. Physics, Utah State University, Logan, UT, 2010.
[8] G. Wilson and J.R. Dennison, "Approximation of Range in Materials as a Function of Incident Electron Energy," submitted to *IEEE Trans. Plasma Sci.*
[9] RC Hoffmann and JR Dennison, "Methods to Determine Total Electron-Induced Electron Yields Over Broad Range of Conductive and Nonconductive Materials," *Proc. of 11th Spacecraft Charging Tech. Conf.*, Albuquerque, NM, 2010.
[10] J.R. Dennison, C. Thomson, J. Kite, V. Zavyalov, and J. Corbridge, "Materials characterization at Utah State University: facilities and knowledgebase of electronic properties of materials applicable to spacecraft charging," in *Proc. of 8th Spacecraft Charging Tech. Conf.*, NASA Marshall Space Flight Center, Huntsville, Al, 2003.
[11] W.Y. Chang, N. Nickles, J.R. Dennison, and C.D. Thomson, "An Improved Database of Electronic Properties of Spacecraft Materials for Modeling of Spacecraft Charging," in *Proc. of 7th Spacecraft Charging Tech. Conf.*, Noordwijk, The Netherlands, 2000.
[12] C.D. Thomson, V. Zavyalov, and J.R. Dennison, "Instrumentation for Studies of Electron Emission and Charging from Insulators," in *Proc. of 8th Spacecraft Charging Tech. Conf.*, NASA Marshall Space Flight Center, Huntsville, Al, 2003.
[13] J. Brunson, "Hopping Conductivity and Charge Transport in Low Density Polyethylene," Ph.D. Dissertation, Dept. Physics, Utah State University, Logan, UT, 2010.
[14] M. Thorne, "Background radiation: natural and man-made," *J. of Radiological Protection*, vol. 23, p. 29, 2003.
[15] J.R. Dennison, J. Gillespie, J. Hodges, R. Hoffmann, J. Abbott, A. Hunt, and R. Spalding, "Radiation Induced Conductivity of highly-Insulating Spacecraft Materials," in *Am. Inst. of Physics Conf. Proc. Series*, pp. 203-208, Melville, NY, 2009.
[16] R. Hoffmann, J. Dennison, C. Thomson, and J. Albretsen, "Low-Fluence Electron Yields of Highly Insulating Materials," *IEEE Trans. Plasma Sci.*, vol. 36, pp. 2238-2245, 2008.
[17] M. Chung and T. Everhart, "Simple calculation of energy distribution of low energy secondary electrons emitted from metals under electron bombardment," *J. of Appl. Phys.*, vol. 45, p. 707, 1974.
[18] N. Nickles, R. Davies, and J.R. Dennison, "Applications of Secondary Electron Energy-and Angular-Distributions to Spacecraft Charging," in *Proc. of 6th Spacecraft Charging Tech. Conf.*, AFRL Science Center, Hanscom AFB, MA, pp. 275-280, 1998.
[19] L. Reimer, "Scanning electron microscopy: physics of image formation and microanalysis," *Measurement Science and Technology*, vol. 11, p. 1826, 2000.
[20] J.L. Hodges, R. Hoffmann and J.R. Dennison, "*In Situ* Measurements of Electron Beam Induced Surface Voltage of Insulators," submitted to *IEEE Trans. Plasma Sci.*
[21] J. Cazaux, "Some Considerations on the Secondary Electron Emission, D, from E Irradiated Insulators," *J. Appl. Phys.* **85**, 1137, 1999.
[22] J. Cazaux,"Scenario for Time Evolution of Insulator Charging under Various Focused Electron Irradiations," *J. Appl. Phys.* **95**, 731, 2003.
[23] A. Melchinger and S. Hofmann, "Dynamic Double Layer Model: Description of Time Dependent Charging Phenomena in Insulators under Electron Beam Irradiation," *J. Appl. Phys.* **78**, 6224, 1995.
[24] X.D. Meyza, Goeuriot, C. Guerret-Piecourt, D. Treheux, and H. Fitting, "Secondary Electron Emission and Self-Consistent Charge Transport and Storage in Bulk Insulators: Application to Alumina," *J. Appl. Phys.* **94**, 5384, 2003.

Ryan Hoffmann received B.S. and MS degrees in physics from Utah State University (USU), Logan, in 2005 and 2010, respectively. He was the lead Research Scientist in the USU Materials Physics Group from 2005 to 2010. He is currently a Research Physicists with the Space Vehicles Directorate at the Air Force Research Laboratory (AFRL) in Albuquerque, NM.

J. R. Dennison received the B.S. degree in physics from Appalachian State University, Boone, NC, in 1980, and the M.S. and Ph.D. degrees in physics from Virginia Tech, Blacksburg, in 1983 and 1985, respectively. He was a Research Associate at the University of Missouri-Columbia before moving to USU, Logan, in 1988. He is currently a Professor of physics with USU, where he leads the Materials Physics Group. He has worked in the area of electron scattering for his entire career and has focused on the electron emission and resistivity of materials related to spacecraft charging for the two decades.